Sedimentary Geology 329 (2015) 177–187

Contents lists available at ScienceDirect

Sedimentary Geology

journal homepage: www.elsevier.com/locate/sedgeo

Habitat heterogeneity reflected in mesophotic reef sediments

D.K. Weinstein [a,*], J.S. Klaus [b], T.B. Smith [c]

[a] Rosenstiel School of Marine and Atmospheric Science, University of Miami, 4600 Rickenbacker Causeway, Miami, FL 33149, USA
[b] Department of Geological Sciences, University of Miami, Cox Science Building 1301 Memorial Dr., Coral Gables, FL 33124, USA
[c] Center for Marine and Environmental Studies, University of the Virgin Islands, 2 John Brewer's Bay, St. Thomas, Virgin Islands 00802, USA

ARTICLE INFO

Article history:
Received 2 May 2015
Received in revised form 8 July 2015
Accepted 9 July 2015
Available online 17 July 2015

Editor: Dr. B. Jones

Keywords:
Mesophotic coral reefs
Sedimentary facies
U.S. Virgin Islands
Bioerosion
Stable isotopic analysis

ABSTRACT

Modern reef sediments reflect the physical and chemical characteristics of the environment as well as the local reef fauna. Analysis of sedimentary reef facies can thus provide a powerful tool in interpreting ancient reef deposits. However, few studies have attempted to differentiate sedimentary facies in mesophotic coral ecosystems, low light habitats defined as residing 30–150 m below sea level. The low-angle shelf mesophotic coral ecosystem south of the northern U.S. Virgin Islands (USVI) consists of reefs with different structural characteristics ideal for studying the relationship between habitat variability and sedimentary facies. Textural, compositional, and geochemical analyses of surface sediments were used to identify mesophotic reef subfacies associated with distinct benthic communities and structural habitats. Sediment grain composition and bulk geochemistry were found to broadly record the distribution and abundance of coral and macroalgae communities, foundational mesophotic reef benthic organisms. Overall, sediment composition was found to be a good indicator of specific reef environments in low-angle mesophotic reef habitats. Sedimentological analyses indicate that hydrodynamic forces do not transport a significant amount of allochthonous sediment or potentially harmful terrigenous material to USVI mesophotic reefs. Episodic, maximum current velocities prevented deposition of most silt-size grains and smaller, but biological processes were found to have a greater influence on subfacies partitioning than hydrodynamic processes. Results provide a new analog for studies of ancient mesophotic coral ecosystem geological history and document the relationship between mesophotic reef subfacies, structural complexity, and habitat heterogeneity. They also demonstrate how mesophotic reefs along the same shelf system do not always share similar sedimentary characteristics and thus record a diverse set of ecological and environmental conditions.

1. Introduction

Studies documenting the taxonomic richness of mesophotic coral ecosystems (MCEs) suggest that biodiversity is a major ecosystem attribute (Cerrano et al., 2010; Lesser et al., 2010; Bridge et al., 2012). Along with macroalgae and sponges, the benthic coverage of mesophotic reefs (30–150 m deep) is dominated by light-dependent scleractinian corals (Lesser et al., 2009). As a photo-adaptation to reduced illumination, mesophotic corals commonly display an overall platy morphology (Fricke et al., 1987; Lesser et al., 2010) similar to what has been found throughout the scleractinian fossil record in environments interpreted as calm and deep (Rosen et al., 2000). The plasticity of modern coral for altering algal symbiosis reliance (Baker et al., 2004) may have evolved early in scleractinian history (Stanley and Fautin, 2001) and affected their ability to survive major extinction events (Veron, 1995). Sedimentary facies analyses have been conducted on a number of ancient mesophotic reef systems (Mesolella et al., 1970; Insalaco, 1996; Dill et al., 2012; Mateu-Vicens et al., 2012; Abbey et al., 2013; Novak et al., 2013; Mihaljević et al., 2014). However, few detailed modern analog studies exist to improve interpretations of ancient MCE reef deposits, and no study has analyzed sediment from multiple mesophotic reef habitats on a low-angle carbonate platform. This limits our knowledge of mesophotic reef evolutionary history and the origins of reef biodiversity.

In shallow reef environments, biodiversity is promoted by ecologically diverse habitats fostered by a spectrum of tidal and wave energy conditions and by habitat modifying species that increase structural complexity, alter hydrodynamics, and increase overall habitat surface area (Connell, 1978; Roberts and Ormond, 1987; Bruno and Bertness, 2001). Structural complexity increases biodiversity and habitat heterogeneity by providing areas with reduced environmental stress needed

Abbreviations: MCE, mesophotic coral ecosystem; USVI, United States Virgin Islands; ADCPs, Acoustic Doppler Current Profilers; ANOVA, one-way analysis of variance; HSD, Honestly Significant Difference; TCRMP, US Virgin Islands Territorial Coral Reef Monitoring Program; NMDS, non-metric multidimensional scaling.

Study site abbreviations: D1, Hillock Basin; D2, Deep Patch; D3, Primary Bank; D4, Secondary Bank; M5, Mid-shelf Patch; S6, Fringing Patch.

* Corresponding author at: Department of Biology, Chemistry, and Marine Science, University of the Ryukyus, 1 Senbaru, Nishihara, Okinawa 903-0213, Japan. Tel.: +81 80 648 48096, +1 301 775 8250; fax: +1 305 421 4632.

E-mail addresses: dweinstein@rsmas.miami.edu (D.K. Weinstein), jklaus@rsmas.miami.edu (J.S. Klaus), tsmith@uvi.edu (T.B. Smith).

http://dx.doi.org/10.1016/j.sedgeo.2015.07.003
0037-0738/

for other organisms to thrive (Thompson et al., 1996) and by improving propagule retention (Eckman et al., 1989). Direct correlations between habitat heterogeneity, fish diversity, and shallow-water reef structural complexity (Roberts and Ormond, 1987; Dustan et al., 2013) and the negative affect global warming is projected to have on reef rugosity (Bozec et al., 2014) emphasize the importance of protecting reef architectural complexity (Dryden et al., 2012). However, little is known about the role of habitat heterogeneity and structural complexity in mesophotic reefs, including their relationship to sedimentary processes and the extent that depositional processes can identify distinct habitats.

The mesophotic reefs of the northern U.S. Virgin Islands (USVI) developed on a low-angle reefal margin that provides space for differing architectural features. Here we present a detailed characterization and interpretation of sediment found within distinct mesophotic reef habitats. Our objectives were to: (1) resolve if low gradient shelf mesophotic reef systems produce recognizable sedimentary facies that reflect structurally distinct reef habitats; and (2) determine the significance of these potential facies differences in terms of biological and hydrodynamic processes. The ability to identify causes and indicators of habitat heterogeneity and structural complexity in modern MCEs is a critical first step in understanding the evolution, development, and maintenance of these attributes in ancient reef systems and the origins of modern biodiversity patterns (Flügel and Flügel-Kahler, 1992; Renema et al., 2008; Morsilli et al., 2012).

2. Materials and methods

2.1. Study sites

Four upper mesophotic (30–60 m) reef habitats (sites D1–D4) with different geomorphology and biological characteristics (described by Smith et al., 2010) were sampled from the Red Hind Marine Conservation District and Grammanik Bank, located on the Puerto Rican shelf, 9.9–15.2 km south of St. Thomas, USVIs (Fig. 1). Two additional reefs (sites M5 and S6) were sampled for shallow-water comparison. Coral cover varied depending on habitat, but approximately 66.8% of the Red Hind Marine Conservation District was composed of adjacent mesophotic coral reefs shallower than 50 m in 2007 (Smith et al., 2010). *Orbicella* spp. was the dominant coral type in the Red Hind Marine Conservation District with a relative coral cover greater than 90%, although Smith et al. (2010) still found high hard coral species richness (37 scleractinian coral and hydrocoral species).

The sites at the narrow (<0.5 km) Primary Bank (D3) and the wider (>1.5 km) Secondary Bank (D4) are the shallowest mesophotic reef study sites (39.0 m and 30.7 m, respectively), have the highest coral cover (>30%), and are geographically closest to the Anegada Passage. The site at the Hillock Basin (D1), north of the Secondary Bank, is located on a deeper (44.5 m) flat expanse, partially composed of thousands of semi-conical knolls. Eastward from the hillocks are a series of low-relief "patches" with low coral cover and abundant rhodolith growth, one of which hosts the selected Deep Patch site (D2) at 41.1 m. The sites at the Mid-shelf Patch (M5) and the Fringing Patch (S6) are closer to shore than their deep-reef counterparts (.08–1.1 km) and reside at depths of 21.0 m and 9.0 m, respectively. Benthic cover (protocol after Smith et al., 2008, 2010) and rugosity (3 m chains; Luckhurst and Luckhurst, 1978) were obtained from the United States Virgin Islands Territorial Coral Reef Monitoring Program (TCRMP). Table 1 displays site average benthic coverage and rugosity measurements from 2012, except for benthic cover at D1 and D2 (recorded in 2007 and 2013, respectively), and rugosity at D3 and M5 (recorded in 2011). The maximum number of transects conducted per site (monthly or episodically, depending on monitoring protocol) during the indicated year were used to calculate the most representative average benthic coverages.

In August 2011, technical divers collected 3–6 replicate samples from the top 3 cm of sediment at each study site (n = 28). All samples were washed with distilled water and dried prior to analysis. Representative living framework samples of *Orbicella* spp. were taken near three of the mesophotic reef sites (D1, D3, D4) for isotopic comparison to bulk sediments. Sediment samples from sites D2, D3, and D4 were collected in the vicinity of Nortek Aquadopp Acoustic Doppler Current Profilers

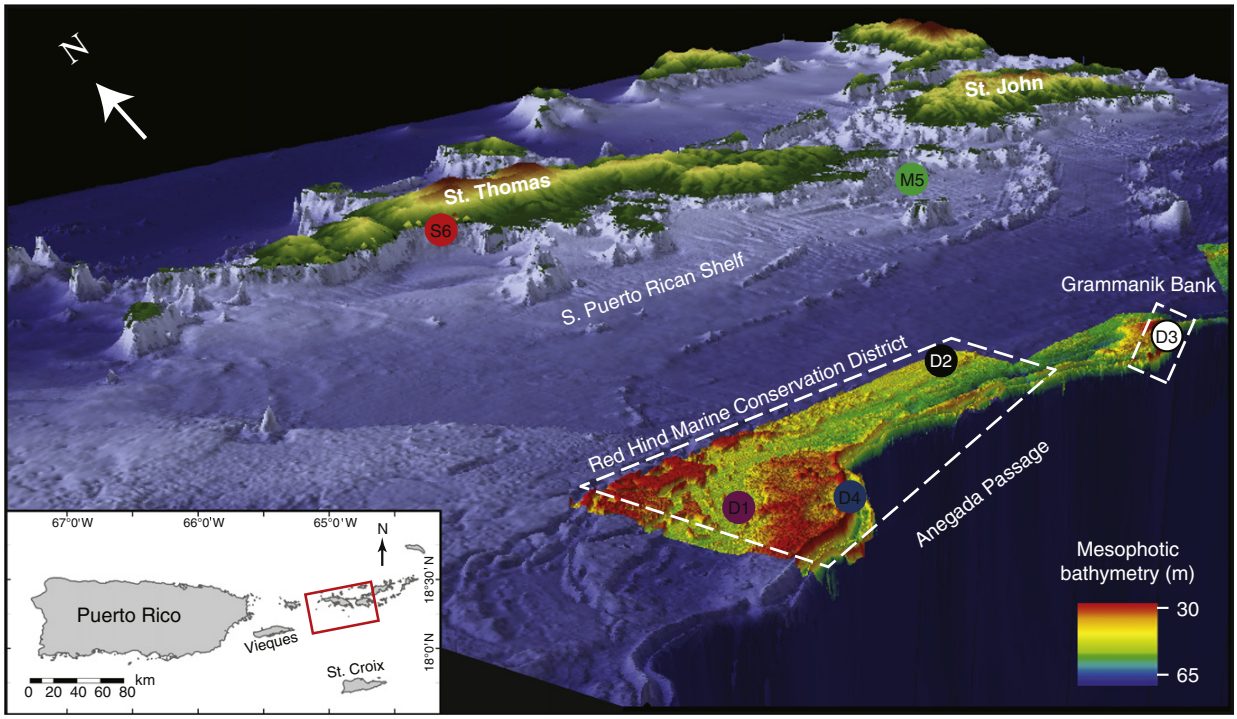

Fig. 1. South Puerto Rican Shelf, with inset marking study location. Multi-beam bathymetry 1 m resolution (20× vertical exaggeration). Study sites include: Hillock Basin (D1); Deep Patch (D2); Primary Bank (D3); Secondary Bank (D4); Mid-shelf Patch (M5); shallow Fringing Patch (S6). 'D' = Mesophotic "deep", 'M' = Mid-shelf, and 'S' = Shallow.

Table 1
Bathymetry, benthic coverage, rugosity, current velocity, and general description of study sites. Rugosity was calculated from 3 transects per site in 2012 (except at D3 and M5, obtained in 2011). Benthic coverage is reported as the average values from the indicated number of transects conducted in 2012 (except D1 and D2, obtained in 2007 and 2013, respectively). Site average spring-neap tidal cycle maximum current velocity ($\overline{CV}_{max}$) and mean current velocity ($\overline{CV}_{mean}$), from 1 February 2008 to 31 January 2009, except at D4. Values are reported with ± 1 standard error. N/A = unavailable data.

Geomorphic site/ depth (m)	Rugosity	% cover		# of transects	Average annual tidal cycle (cm/s)	Site description
		Live coral	Macroalgae Coralline Algae		$\overline{CV}_{max}$ $\overline{CV}_{mean}$	
Hillock Basin (D1) 44.5	1.84 ± 0.44	12.99 ± 4.18[a]	45.42 ± 1.74[a] 15.10 ± 2.22[a]	3[a]	34.84 ± 4.04 7.07 ± 0.75	Flat sand and sparse coral expanse 2.3 km^2 with over 10,000 coral "hillock" semi-conical knolls ~5-20 m diameter with 2-10 m of vertical relief.
Deep Patch (D2) 41.1	1.13 ± 0.02	1.79 ± 0.81[b]	54.01 ± 6.56[b] 12.36 ± 3.20[b]	3[b]	18.83 ± 0.97 6.92 ± 0.32	Semi-conical (>0.5 km diameter), <5 m of vertical relief. High rhodolith cover and low cover of ephemeral coral opportunists. Near other isolated patches.
Primary Bank (D3) 39.0	2.62 ± 0.63[c]	32.20 ± 2.59	34.28 ± 1.40 5.89 ± 0.93	6	19.53 ± 1.45 7.22 ± 0.38	Southernmost semi-continuous mesophotic reef parallel and adjacent to Anegada Passage for >1 km. Narrow (<0.5 km) width bank with >5 m of vertical relief.
Secondary Bank (D4) 30.7	1.55 ± 0.14	33.73 ± 2.54	36.80 ± 1.64 8.94 ± 1.03	6	24.24 ± 3.31[d] 7.57 ± 0.20[d]	North, more continuous, wider (>1.5 km), and parallel to Primary Bank for >1 km, with a broader sloping northern edge and >5 m of vertical relief.
Mid-shelf Patch (M5) 21.0	1.18 ± 0.04[c]	18.26 ± 0.60	54.20 ± 2.68 2.04 ± 0.36	42	N/A	Large mid-shelf isolated flat-topped patch surrounded by rhodoliths and sand.
Fringing Patch (S6) 9.0	1.24 ± 0.01	3.19 ± 0.76	37.04 ± 3.71 0.34 ± 0.34	3	N/A	Isolated fringing patch ~30 m offshore in Perseverance Bay. Sparse coral community impacted by terrestrial runoff.

[a] Data collected in 2007.
[b] Data collected in 2013.
[c] Data collected in 2011.
[d] based on data obtained from 20 May to 26 September 2014.

(ADCPs), which recorded hourly current velocities 1.5–2.5 m above the seafloor with a 1 m swath. ADCP measurements from a nearby (1.36 km) site (Hind Bank; from Smith et al., 2010) were used as a proxy for the Deep Patch (D2) site. The average of each spring–neap tidal cycle current velocity mean and maximum were calculated from 1 February 2008 to 31 January 2009 for sites D1–D3 (Table 1), and subdivided to distinguish summer (May–November) and winter (December–April) trends (Electronic Supplementary Material, ESM Table 1). Two spring–neap tidal cycles were estimated per month; the first 15 days of the month and the remaining days of the month. Secondary Bank (D4) current data were only available from 20 May to 26 September 2014 (Table 1). Assuming a bed roughness length (z_0) of 0.3 mm (Soulsby, 1997), the von Karman–Prandtl law-of-wall equation (with $\kappa = 0.4$) was used to calculate shear velocity (u_*) for each hourly recorded current velocity. The equation was then used to recalculate the site average spring–neap tidal cycle current velocity means and maximums to account for boundary layer conditions z = 25 mm above the seafloor.

2.2. Sediment composition

To quantify sediment composition, three sediment samples per site were passed through a 2 mm mesh sieve, impregnated with resin, and thin-sectioned. Standard point-count analysis was conducted on a minimum of 300 points per thin section (identified as a statistically sufficient number of points, when following the rarefaction curve methodology of Pandolfi et al., 1999) using the JmicroVision program (Roduit, 2008). Grain classifications were based on literature descriptions (Ginsburg, 1956; Pusey, 1975; Scholle, 1978; Adams et al., 1984). Data were corrected with the arcsin transformation, and one-way analysis of variance (ANOVA) tests were conducted to determine significant univariate differences between sites. Specific pair-wise differences were identified using Tukey's Honestly Significant Difference (HSD) multiple comparison test. Pearson's correlations were used to compare sediment types with depth. Benthic coverage data lacked a normal distribution so Spearman's correlations were used to compare the relative sample (3 per site) percentage of coral, calcareous green algae, and coralline algae grains with the equivalent average benthic cover (coral and algae) at the sample collection sites (samples from the same sites were compared to the same site average benthic cover values). For this study, calcareous green algae was used as a proxy for macroalgae in the fossil record. Spearman's correlation was also used to compare the relative sample percent of mesophotic reef sediment coral grains with adjusted bioeroding parrotfish biomass, which lacks a normal distribution (from Weinstein et al., 2014). Statistical testing was conducted using the program R version 3.0.3 (R Core Team, 2014). Overall site differences in sediment composition type were visually assessed by non-metric multidimensional scaling (NMDS) of the Bray–Curtis dissimilarity index using the PAST statistical software package (Hammer et al., 2001).

2.3. Stable carbon and oxygen isotopes

Sediments from 26 samples (2 samples were depleted for other analyses) that passed through a 2 mm mesh sieve were ground in preparation for analysis. The bulk stable oxygen and carbon isotope ratios of both sediment and coral samples were determined by the common acid bath method (Swart et al., 1991). Phosphoric acid dissolution of ground samples (~0.5–1 mg) produced gas analyzed with a Finnigan-MAT 251 mass spectrometer at the University of Miami Stable Isotope Laboratory. Results were corrected for isobaric interferences (Craig, 1957) and reported relative to the standard Vienna Pee Dee Belemnite. Replicate error analysis of inorganic $\delta^{13}C$ and $\delta^{18}O$ standards produced a standard deviation <0.1‰. Significant univariant site differences were tested using one-way ANOVA and Tukey's HSD tests. Pearson's correlations were used to compare $\delta^{18}O$ with $\delta^{13}C$, and also to compare isotope concentrations with axis 1 of the grain composition NMDS ordination. Linear regression was used to compare surface sediment bulk isotopic composition directly with the percent of coral grains in corresponding sediments. The program R version 3.0.3 (R Core Team, 2014) was used for all isotope statistical analysis.

2.4. Grain size analysis

Standard wet sieving techniques (mesh sizes 4, 2, 1, 0.5, 0.25, 0.125, and 0.63 mm) for grain size analysis (Folk, 1974) were used on ~5–20 g

of all samples (n = 28). Standard textural parameters (mean grain size, sorting, skewness, and kurtosis) of each sample were obtained using the program GRADISTAT (Blott and Pye, 2001) when assuming all sediment that passed through the smallest sieve (0.63 mm) could be grouped into a bin with a mesh size of 0. 31 mm (5 ϕ). Site average grain size distributions were obtained by taking the average of each individual mesh bin per site, and then calculating the relative percent of that bin to the total. One-way ANOVA and Tukey's HSD tests on sample standard textural parameters were used to assess site variance with R version 3.0.3 (R Core Team, 2014).

To investigate allochthonous sediment deposition potential, settling velocities (w_s) of unconsolidated suspended sediment grains with specific diameters were converted to equivalent spherical quartz settling velocities with the Gibbs et al. (1971) equation, multiplied by a corrective factor ($R_D = 0.98$; Komar, 1981). Average grain density was set to $\rho_S = 1850$ kg/m^3 (Kench and McLean, 1996), dynamic viscosity was set to $\mu = 9.037 * 10^{-4}$ Pa∗s (calculated from El-Dessouky and Ettouney, 2002), and fluid density was set to $\rho_f = 1022.9$ kg/m^3 (calculated from Millero et al., 1980). Constants were calculated using a representative depth, temperature, and salinity of 40.5 m, 27.9 °C, and 35.577 ppt. The calculated w_s for unconsolidated fine sand (125 μm), very fine sand (104.4 μm), and grains equivalent in size to sponge chips (mean diameter of 40 μm; Rützler, 1975) were 0.6582 cm/s, 0.4777 cm/s, and 0.0768 cm/s, respectively. As these unconsolidated grain sizes were relatively small, modeling potential for deposition of well sorted grains in the water column could be simplified by applying equations derived for regular quartz grains, assuming similar shape (Prager et al., 1996). Settling velocities were divided by shear velocity (u_*) to determine the percent of time that currents were slow enough to permit the fall of suspended particles (when $w_s/u_* \geq 1.25$; Cheng and Chiew, 1999), assuming minimal baffling for depths ≤2.5 m above the seafloor.

2.5. Currents of removal

Sieve-based grain size analysis was used to provide better comparisons with ancient reefal deposit analyses. Application of carbonate sediment sieve analysis is questionable, however, when interpreting hydrodynamic processes (see Kench and McLean, 1997). Therefore a "currents of removal" approach (Kench, 1998) for determining potential mobility was used to examine surface sediment erosion and transport. To estimate potential mobility (Kench, 1998) and compare with previous evaluations of carbonate sieve-based analysis (Kench and McLean, 1997), the sieve sizes used in this study were converted to equivalent spherical quartz settling velocities with the Gibbs et al. (1971) equation, applying the same corrective factor and constants from earlier analyses. After converting sieve size values to the standard settling velocity chi (χ) parameter (May, 1981), the original site average weights associated with the equivalent sieve settling velocities were plotted as mean cumulative settling velocity distribution curves for each site.

When defining threshold velocity as the average velocity recorded 25 mm above a flume bottom needed to move 50% of a heterogeneous reefal sediment fraction, Kench and McLean (1996) suggested sediment fraction mobility could be characterized by a mean settling velocity. The threshold curve derived by Kench and McLean (1996) was assumed to be an accurate proxy because USVI sediment had similar compositional characteristics to the sediment used to develop the threshold curve. Recalculated average spring–neap tidal cycle current velocity maximum values ($\overline{CV}_{max}$; 25 mm above the seafloor) were plotted as the independent variable of an asymptotic convex regression equation fitted to the threshold curve from Kench and McLean (1996), such that:

$$w_s = -\ln\left(\frac{v - 16.310701}{104.115782}\right) * 1.780639, \quad \text{where } v = \text{velocity (cm/s)}.$$

The resultant dependent variable, in chi units, approximates the largest mean particle settling velocity (representing a particular heterogeneous sediment fraction) that can be entrained at the average spring–neap tidal cycle current velocity maximum. The largest mean settling velocity (in χ) was plotted vertically on the cumulative settling velocity distribution curve from the same site so that the line and curve intercepted. The percent of settling distribution fractions above the intercept is defined as the site surface sediment potential mobility at the site average spring–neap tidal cycle current velocity maximum (Kench, 1998). This procedure assumes all recalculated current velocities are as unobstructed by surrounding topography as the original measurements, minus bed roughness.

To estimate potential mobility frequency, the cumulative distribution curves were used to determine settling velocities associated with 50%, 10%, and 2.5% potential mobility fractions. The associated settling velocities were input into the asymptotic convex regression equation to calculate equivalent threshold current velocities (in cm/s). The velocities were then compared with hourly recorded site ADCP currents, converted to z = 25 mm above the seafloor to account for boundary layer conditions, to determine the percent of hours in a year that currents were greater than or equal to velocities needed for the different potential mobility fractions.

3. Results

3.1. Grain composition

Twelve sediment-type categories were identified (Fig. 2a, ESM Table 2): coral; micritic grains; composite micritic grains; mollusk; foraminifera; calcareous green algae (primarily *Halimeda*); coralline algae; echinoderm; bryozoan; terrigenous; carbonate mud/silt; and other (spicules, fecal pellets, worm tubes, unattached cements, and unidentifiable). Classifications were intended to describe the dominant grain type each point resided on, despite the presence of intraskeletal cements or attached intragranualar cements. Coral was the most common category in all but the Deep Patch samples. Terrigenous material was not found at any mesophotic sites, but constituted ≥9% of the sediment from all shallow Fringing Patch site samples and a trace amount from the Mid-shelf Patch site. Average echinoderm, bryozoan, and carbonate mud/silt sediment-type concentrations were <5% per site.

Analysis of variance indicated statistically significant differences when comparing all sites and when just comparing mesophotic sites, respectively for: coral ($F_{5,12} = 15.88$, $p < 0.001$; $F_{3,8} = 47.49$, $p < 0.001$); micritic grains ($F_{5,12} = 7.92$, $p = 0.002$; $F_{3,8} = 14.67$, $p = 0.001$); foraminifera ($F_{5,12} = 16.68$, $p < 0.001$; $F_{3,8} = 30.59$, $p < 0.001$); and calcareous green algae ($F_{5,12} = 10.50$, $p < 0.001$; $F_{3,8} = 29.38$, $p < 0.001$). Significant differences were also found in the relative abundance of coralline algae between mesophotic sites ($F_{3,8} = 4.06$, $p = 0.050$). Pair-wise comparison results are displayed in Table 2. NMDS ordination of the Bray–Curtis dissimilarity matrix visually indicated differences in grain composition among the study sites (Fig. 2b) and was supported statistically by one-way analysis of similarity ($r = 0.7004$, $p = 0.0001$). Axis 1 of the NMDS ordination showed an overall gradient from sites with sediment composition dominated by coral grains (D3, D4, M5, and S6) to sites with sediment composition dominated by foraminifera, calcareous green algae, and micritic grains (D1 and D2). Fringing Patch sediment was distinguishable from other sites by an abundance of terrigenous material and greater amounts of mud/silt. Deep Patch sediment was distinguishable by a greater abundance of calcareous green algae and foraminifera-derived grains and fewer coral-derived grains.

Of all grain types, only foraminifera grain abundance was found to have a significant linear relationship with water depth (strong negative correlation; $n = 18$, $r = -0.86$, $p < 0.001$). Among mesophotic sites, strong significant correlations were found between abundance of coral sediment grains and benthic coral cover ($n = 12$, $\rho = 0.972$, $p < 0.001$) and between abundance of calcareous green algal sediment grains and macroalgae benthic cover ($n = 12$, $\rho = 0.607$, $p = 0.036$) (Fig. 2c). Strong, significant correlations were also found between the

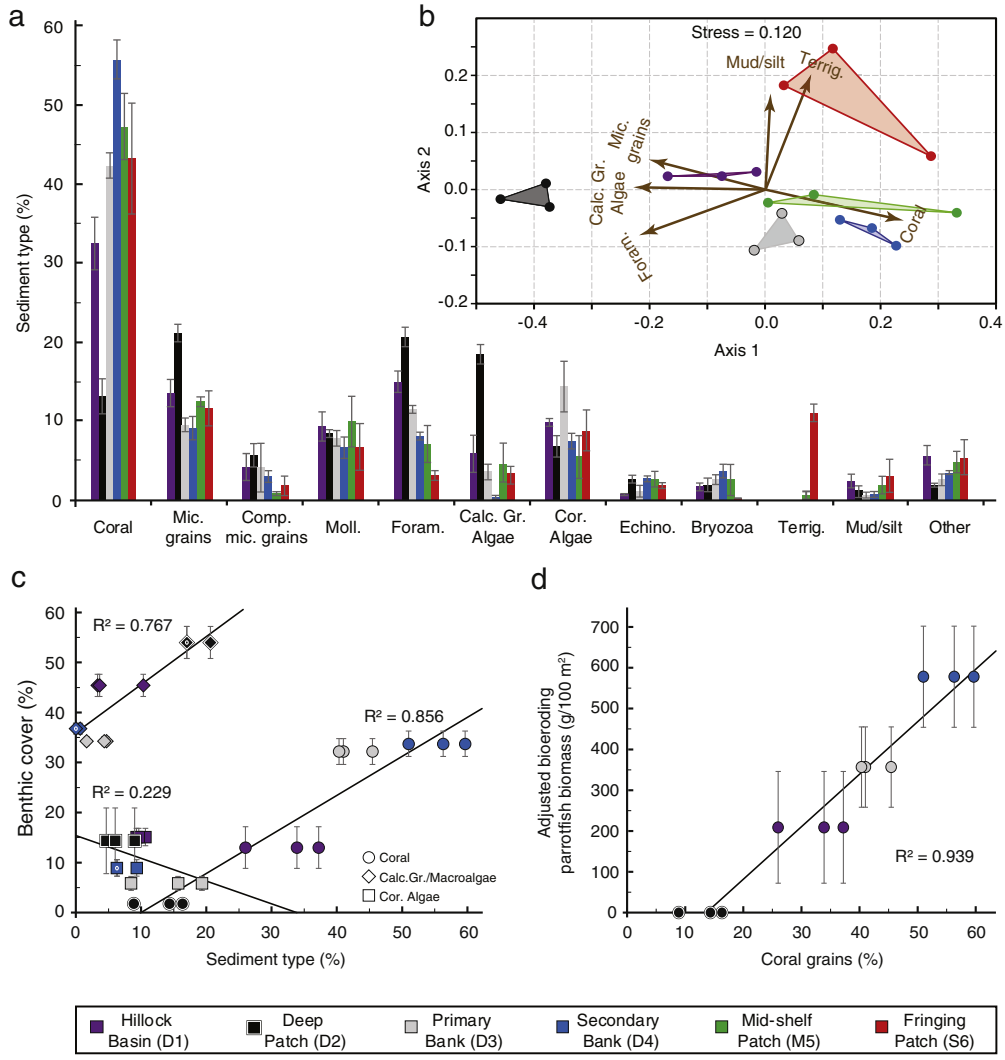

Fig. 2. Surface sediment composition. (a) Average percent of constitute sediment type per site. (b) Non-metric multidimensional scaling (NMDS) ordination. Arrow length indicates correlation of sediment type to sample ordination. (c) Correlation between percent of carbonate sediment type (coral, calcareous green algae, and coralline algae) and corresponding average site benthic cover, as given in Table 1. Clear circles on symbols indicate that a second nearly identical data point is located at the same position. (d) Correlation between percent of coral grains in bulk mesophotic reef sediment and adjusted bioeroding parrotfish biomass, as defined by Weinstein et al., 2014. Key at bottom indicates sites for all figures. Error bars equal to one standard error. Mic. = Micritic, Comp. = Composite, Moll. = Mollusk, Foram. = Foraminifera, Calc. = Calcareous, Gr. = Green, Cor. = Coralline, Echino. = Echinoderm, Terrig. = Terrigenous.

abundance of coral sediment grains and adjusted bioeroding parrotfish biomass ($n = 12$, $\rho = 0.972$, $p < 0.001$) (Fig. 2d).

3.2. $\delta^{13}C$ and $\delta^{18}O$ isotopic composition

Bulk surface sediment stable isotope values (ESM Table 3) ranged from −2.22‰ to −0.54‰ for oxygen ($\delta^{18}O$) and from 0.93‰ to 3.62‰ for carbon ($\delta^{13}C$). Both showed statistically significant differences between site means ($\delta^{18}O$: $F_{5,20} = 30.99$, $p < 0.001$; $\delta^{13}C$: $F_{5,20} = 44.28$, $p < 0.001$). Specific pair-wise differences are displayed in Table 2. A significant positive correlation was found between $\delta^{18}O$ and $\delta^{13}C$ ($n = 26$, $r = 0.829$, $p < 0.001$) (Fig. 3a). Furthermore, $\delta^{18}O$ and $\delta^{13}C$ values were generally related to depth, with more negative values found at shallow sites and positive values at deeper sites. To investigate potential relationships between bulk sediment stable isotope composition and sediment type, axis 1 from NMDS ordination analysis (primarily representing relative composition of coral, foraminifera, calcareous green algae, and micritic grains) was plotted versus sample bulk $\delta^{13}C$ and $\delta^{18}O$. Axis 1 showed a significant negative correlation with both $\delta^{13}C$ ($n = 18$, $r = -0.874$, $p < 0.001$) and $\delta^{18}O$ ($n = 18$, $r = -0.790$, $p < 0.001$). Additionally, the $\delta^{13}C$ and $\delta^{18}O$ of collected bulk mesophotic reef sediments both had significant linear relationships (Fig. 3b) with the percent of coral grains in corresponding sediments ($\delta^{13}C$: $n = 11$, $R^2 = 0.961$, $p < 0.001$; $\delta^{18}O$: $n = 11$, $R^2 = 0.890$, $p < 0.001$). The projected isotopic composition of bulk mesophotic reef sediment with 100% coral composition is consistent with measured isotopic values of the dominant USVI mesophotic corals (Fig. 3b).

3.3. Grain size and hydrodynamics analyses

The site average grain size distributions and site average of each main standard textural parameter are shown in Fig. 4 (see ESM Table 4 for grain size distribution per sample). Sample standard textural parameters did not have any clear linear relationships with collection depth. Site average mean grain size was largest at the Deep Patch site and smallest at the Hillock Basin site (Fig. 4b). All 28 samples were

Table 2
Surface sediment pair-wise analysis results of Tukey's Honestly Significant Difference test, comparing sediment attributes between sites. Values were included when significant ($p < 0.05$). Parentheses indicate test results for which only mesophotic reef sites were considered. Foram. = Foraminifera, Calc. gr. algae = Calcareous green algae.

Site differences		Grain composition				Stable isotopes		Grain size analysis		
		Coral	Micritic grains	Foram.	Calc. Gr. Algae	$\delta^{13}C$	$\delta^{18}O$	Mean	Sorting	Skewness
Mesophotic	Primary Bank: Secondary Bank	(0.045)		(0.063)	(0.030)	<0.001 (<0.001)	0.038 (0.004)			
	Deep Patch: Secondary Bank	<0.001 (<0.001)	0.001 (0.002)	0.003 (<0.001)	<0.001 (<0.001)	<0.001 (<0.001)	<0.001 (<0.001)	(0.024)	(0.030)	0.003
	Hillock Basin: Secondary Bank	0.015 (0.002)		(0.002)	0.037 (0.007)	<0.001 (<0.001)	<0.001 (<0.001)			
	Deep Patch: Primary Bank	0.001 (<0.001)	0.002 (0.002)	0.047 (0.001)	0.009 (0.002)	<0.001 (<0.001)	<0.001 (<0.001)			0.009
	Hillock Basin: Deep Patch	0.016 (0.002)	(0.035)	(0.025)	0.038 (0.007)	<0.001 (<0.001)	0.047 (0.005)	0.001 (<0.001)	(0.036)	0.008
	Hillock Basin: Primary Bank					(0.016)	(0.034)			
Mesophotic / Shallow	Secondary Bank: Fringing Patch								0.018	
	Primary Bank: Fringing Patch			0.005		<0.001	<0.001			
	Deep Patch: Fringing Patch	0.001	0.014	<0.001	0.006	<0.001	<0.001			
	Hillock Basin: Fringing Patch			0.001		<0.001	<0.001		0.021	
	Secondary Bank: Mid-shelf Patch					0.003				
	Primary Bank: Mid-shelf Patch						0.002			
	Hillock Basin: Mid-shelf Patch			0.023			<0.001			
	Deep Patch: Mid-shelf Patch	<0.001	0.027	0.001	0.012	<0.001	<0.001			<0.001
Shallow	Mid-shelf Patch: Fringing Patch					0.045				0.011

primarily composed of sand-sized particles and gravel, with trace amounts of mud (Fig. 4c). On average, all mesophotic reef surface sediments contained <5% mud.

Site average grain size distributions were unimodal at the Deep Patch and Hillock Basin sites and bimodal at the Mid-shelf Patch site, the Fringing Patch site, and the Primary and Secondary Bank sites (Fig. 4a). The primary grain size mode was 0.5–0.3 mm for all sites except the Fringing Patch and Deep Patch sites (1–0.25 mm and 6–3 mm, respectively). The Deep Patch site primary grain size mode was similar to the secondary grain size mode of all other sites with bimodal grain size distributions. Site mean comparisons indicated statistically significant differences between each standard sediment textural parameter (grain size: $F_{5,22} = 5.01$, $p = 0.003$; sorting: $F_{5,22} = 4.73$, $p = 0.004$; skewness: $F_{5,22} = 7.48$, $p < 0.001$; and kurtosis: $F_{5,22} = 3.36$, $p = 0.021$). When comparing only mesophotic sites, significant differences between sites were found for mean grain size and sorting ($F_{3,17} = 9.93$, $p < 0.001$;

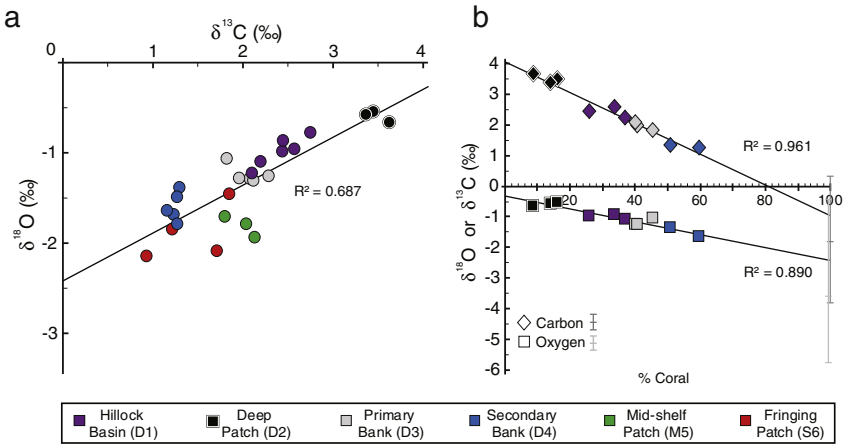

Fig. 3. Bulk sediment isotopic composition. (a) Relationship between bulk sediment stable carbon and oxygen isotopic composition. (b) Relationship between the percent of coral grains in collected mesophotic reef bulk surface sediment and the corresponding bulk sediment stable isotopic composition of oxygen (squares) and carbon (diamonds). Gray vertical lines indicate the average isotopic ranges (with middle line showing mean) obtained from representative living framework *Orbicella* spp. samples. Key at bottom displays site symbols for all figures. Standard error bars for stable isotopic compositions are smaller than symbols.

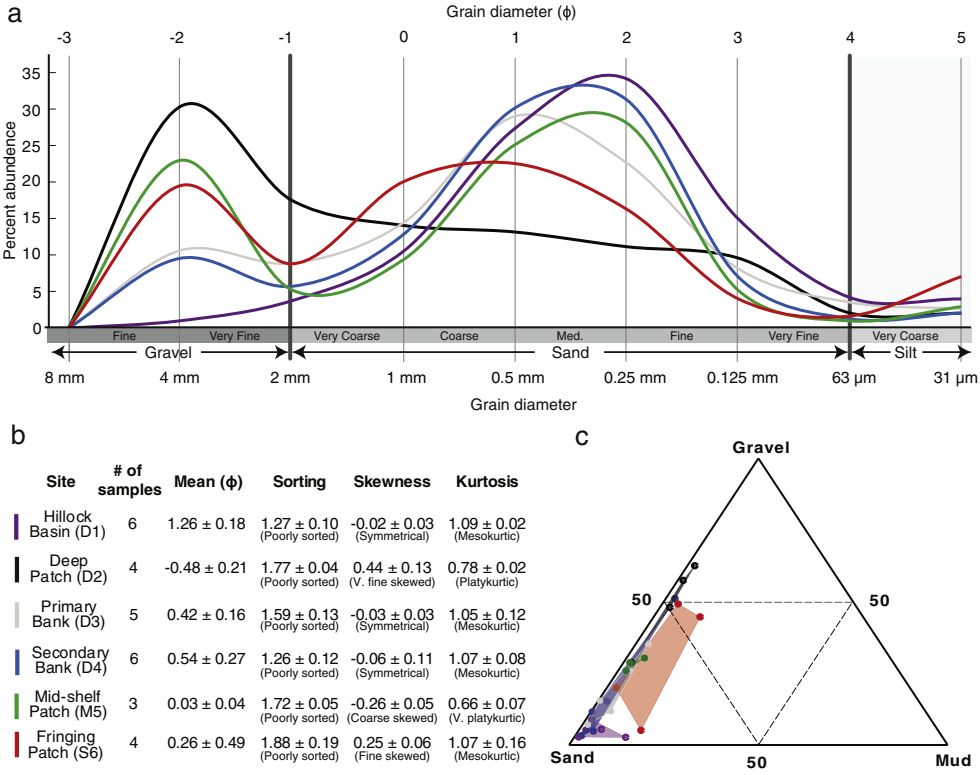

Site	# of samples	Mean (ϕ)	Sorting	Skewness	Kurtosis
Hillock Basin (D1)	6	1.26 ± 0.18	1.27 ± 0.10 (Poorly sorted)	-0.02 ± 0.03 (Symmetrical)	1.09 ± 0.02 (Mesokurtic)
Deep Patch (D2)	4	-0.48 ± 0.21	1.77 ± 0.04 (Poorly sorted)	0.44 ± 0.13 (V. fine skewed)	0.78 ± 0.02 (Platykurtic)
Primary Bank (D3)	5	0.42 ± 0.16	1.59 ± 0.13 (Poorly sorted)	-0.03 ± 0.03 (Symmetrical)	1.05 ± 0.12 (Mesokurtic)
Secondary Bank (D4)	6	0.54 ± 0.27	1.26 ± 0.12 (Poorly sorted)	-0.06 ± 0.11 (Symmetrical)	1.07 ± 0.08 (Mesokurtic)
Mid-shelf Patch (M5)	3	0.03 ± 0.04	1.72 ± 0.05 (Poorly sorted)	-0.26 ± 0.05 (Coarse skewed)	0.66 ± 0.07 (V. platykurtic)
Fringing Patch (S6)	4	0.26 ± 0.49	1.88 ± 0.19 (Poorly sorted)	0.25 ± 0.06 (Fine skewed)	1.07 ± 0.16 (Mesokurtic)

Fig. 4. Grain size analysis. (a) Graph of average grain size distribution per site, with gray shaded area indicating distribution estimates after last sieve bin (63 µm). Gray area could stretch further depending on the size of remaining mud. (b) Average textural parameters per site, ± 1 standard error. (c) Classification of sediments as a ternary diagram. Key on left side of (b) displays site symbols for figures.

$F_{3,17} = 4.68$, $p = 0.015$, respectively). Mesophotic reef sediment skewness and kurtosis did not meet assumptions for ANOVA. Specific pairwise site differences for tested textural parameters are shown in Table 2.

Fine sand grains (diameter = 125 µm) could potentially deposit at the Hillock Basin and Deep Patch sites for 56.45% and 42.92% of all hours in the measured time span, respectively (Table 3). However, less than 1.5% of all hourly current measurements were theoretically conducive for the deposition of unconsolidated grains with average sponge chip diameters. According to potential mobility analysis, site average spring–neap tidal cycle current velocity means were rarely strong enough to entrain unconsolidated reef surface sediment at any of the sites (potential mobility < 4%) but high potential entrainment was possible in response to site average spring–neap tidal cycle current velocity maximums, especially at the Hillock Basin site (Table 3). Conditions necessary to entrain at least a fourth of unconsolidated surface sediment (50% potential mobility) where most frequent at the Hillock Basin site but occurred <3% of the hours in the sampled year (Fig. 5). Comparatively, 2.5% potential mobility frequency of unconsolidated surface sediment at the Hillock Basin was more than four times greater than at the Deep Patch.

Table 3
Potential deposition and potential mobility (PM). Percentage of hours measured in which unconsolidated grains (three representative diameter sizes) would deposit from suspension if initially present 25 mm above the seafloor. Potential mobility analysis is applied to the site average grain size distribution. N/A = unavailable data.

	Geomorphicsites	Grains (µm)	Annual	Summer	Winter
% (hours in a year) of potential deposition	Hillock Basin (D1)	125	58.58%	31.71%	26.87%
		104.4	36.66%	20.24%	16.41%
		40	1.27%	0.64%	0.63%
	Deep Patch (D2)	125	44.95%	15.60%	29.36%
		104.4	25.72%	8.22%	17.50%
		40	0.84%	0.25%	0.59%
	Primary Bank (D3)	125	38.57%	20.76%	17.81%
		104.4	21.67%	11.01%	10.65%
		40	0.50%	0.18%	0.32%
	Secondary Bank (D4)	125		38.75%	
		104.4	N/A	21.90%	N/A
		40		0.71%	
PM (%)	Hillock Basin (D1)	Complete grain size distribution	88.8	95.1	49.0
	Deep Patch (D2)		8.1	14.1	0.1
	Primary Bank (D3)		10.8	10.9	10.8
	Secondary Bank (D4)		N/A	36.0	N/A

3.4. Sedimentary subfacies

The reef surface sediment samples collected in the USVI could all be broadly characterized as a carbonate bioclastic sand. Given their pre-lithified state, the surface samples were further classified into subfacies based on textural and compositional properties. Classification was restricted to two main properties per subfacies. To include all samples, average site composition values were used for samples where thin section analysis was not available. Subfacies descriptions (Table 4) primarily group collected samples into the six different habitat types analyzed in this study. Three of the subfacies included one sample from a different habitat type, and only one sample was absent from its associated main subfacies habitat group.

4. Discussion and conclusions

Significant differences in sediment parameters (Table 2) indicate distinct associations between mesophotic reef habitats with architecturally different characteristics in the U.S. Virgin Islands and

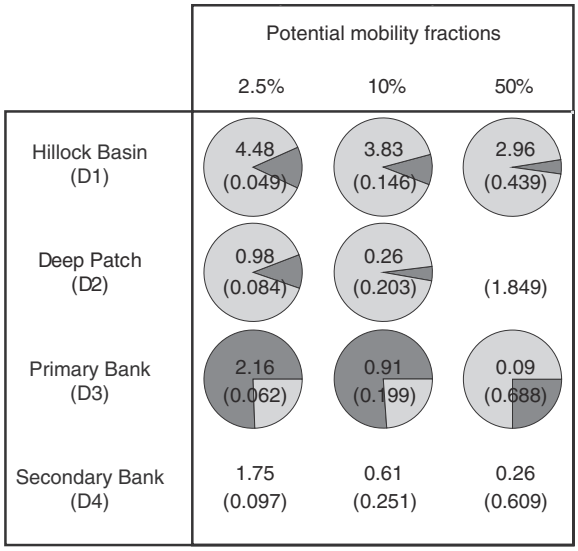

Fig. 5. Percent of hours measured in a year (or all hours measured at D4) for different potential mobility fractions for the site mean settling velocity. Pie chart delineates hour proportions per season (light gray = summer, dark gray = winter). Parentheses indicate the maximum equivalent grain size diameter (mm) that could be entrained for the corresponding potential mobility fraction, calculated from the Gibbs et al. (1971) equation and applying the same corrective factor and constants as explained in the text. No 50% potential mobility graph is presented for the Deep Patch site because conditions were never met. Secondary Bank data only available during summer 2014.

sedimentary subfacies. These imply that sediment composition in this region is a fair indicator of specific mesophotic reef environments, similar to results from Jamaican reefs (Boss and Liddell, 1987; Perry, 1996). The type, size, and chemical composition of reef sediment is controlled through a combination of independent and interacting biological and physical processes. Isolating the effects and interactions of these processes is an important step in using reef sediments as a means to identify and interpret MCE habitat heterogeneity both in modern and ancient reef environments.

4.1. Biological controls

Overall, the mesophotic reef habitats in the USVI experience local sediment production and deposition primarily controlled by biological processes. Mesophotic reef sediment composition broadly records the abundance of two major habitat-forming benthic groups. This record is indicated by significant correlations between sediment types (coral and calcareous green algae) and living benthic cover, as well as by bulk isotopic composition trends (coral generally has the most negative isotopic values and calcareous algae has the most positive isotopic values of reefal skeletal sediment; Gischler et al., 2009). For example, the Deep Patch and the Hillock Basin sites have the lowest mesophotic coral cover and average coral sediment percentages but the highest mesophotic reef macroalgae and average calcareous green algae sediment percentages. These two sites also have the heaviest average stable isotope compositions of analyzed surface sediments. Our conclusion supports the general understanding that carbonate sand composition is largely controlled by the relative abundance of skeletal producers (Basan, 1973) and is similar to results from Jamaican reefs (Boss and Liddell, 1987; Perry, 1996), although these studies did not go into as much detail at mesophotic reef depths. Contrastingly, high coral-grain percentages (>30%) in Florida reefs have been interpreted as resulting from great amounts of dead substrate accessible for bioerosion and to imply that the reef is in rapid decline (Lidz and Hallock, 2000). However, long predicted framework exposure times (Weinstein et al., 2014) and observations of USVI mesophotic reefs suggest an ample supply of accessible, erodible substrate beneath the living platy coral veneer.

Poor sorting of all collected samples may also indicate that study site grain sizes are primarily controlled by biological processes (Scoffin and Tudhope, 1985), but could somewhat result from limitations with sieve-based analysis methodology (Kench and McLean, 1997). Reef sediments often split into discrete size intervals (Folk and Robles, 1964; Basan, 1973; Flood and Scoffin, 1978). The main grain size interval from the USVI mesophotic reef sites corresponds with coral grit (0.5–.25 mm), a dominant fraction identified in other reefal deposits (Folk and Robles, 1964; Garrett et al., 1971). The high coral grit to coarser coral grain size ratio implies longer seafloor exposure (Scoffin, 1992). The primary grain size mode at the Deep Patch is similar to whole *Halimeda* segments (8–4 mm; Folk and Robles, 1964). This follows expectations given that the Deep Patch has a high relative proportion of calcareous green algae-derived surface sediment compared to the other sites.

Table 4
Sedimentary subfacies classifications of USVI surface reef sediments. Bold sample ID numbers indicates samples for which site average grain composition abundances were used for classification purposes. Underlined sample ID numbers indicate samples classified in 2 subfacies. Italicized sample ID numbers indicates samples from a different habitat than the associated geomorphic site. Gray box indicates not all samples from the associated geomorphic site are included in the subfacies. Sample ID numbers begin with site abbreviation code. M_z = sample mean grain size diameter (mm). Sk_I = sample grain size distribution skewness. Calc. gr. algae = Calcareous green algae.

Sedimentary facies	Subfacies	Defining characteristics	Sample ID numbers	Associated geomorphic site/ depth (m)
Carbonate bioclastic sand	Moderate coral rich, medium grained sand	<40% coral, M_z<0.70	**D1.1**, D1.2, **D1.3**, **D1.4**, D1.5, D1.6, *S6.4*	Hillock Basin (D1) 44.5
	Green algae rich coarse grained sand	>15% green algae, M_z>0.70	D2.1, D2.2, D2.3, **D2.4**	Deep Patch (D2) 41.1
	Coral rich, foraminifera rich sand	>40% coral, >10% foraminifera	D3.1, D3.2, **D3.3**, D3.4, **D3.5**, *M5.1*	Primary Bank (D3) 39.0
	Coral rich, green algae poor sand	>40% coral, <1% green algae	**D4.1**, **D4.2**, **D4.3**, D4.4, D4.5, D4.6, *M5.3*	Secondary Bank (D4) 30.7
	Coarsely skewed, terrestrial present sand	coarse to very coarsely skewed (Sk_I<−0.1), >0% terrigenous	M5.1, M5.2	Mid-shelf Patch (M5) 21.3
	Terrestrial rich, muddy sand	>10% terrigenous, >2% mud content	S6.1, S6.2, **S6.3**, S6.4	Fringing Patch (S6) 9.1

Biological processes also control reef sediment textural properties through bioerosion, a dominant reef mechanism for sediment formation and framework alteration (see review by Hutchings, 1986). Parrotfish typically produce sand-sized (0.5–0.125 mm) fecal carbonate sediment (Gygi, 1969; Garrett et al., 1971) similar to grain size modes common in USVI reefs (Fig. 4a). Parrotfish activity may also be the cause of the second most common grain size mode (6–3 mm) at the shallowest four study sites (D3, D4, M5, and S6) by detachment of coral framework not actually ingested. The relative absence of gravel-sized grains at the Hillock Basin likely reflects the lower adjusted biomass of bioeroding parrotfish (Fig. 2d) compared to the higher coral cover mesophotic reef bank habitats. Coarser grains, a relatively flat bathymetric profile, and low structural complexity (Table 1) are reflected in the significant negative skewness of Mid-shelf Patch sediment (Jordan, 1973).

4.2. Hydrodynamic controls

Low-angle shelf mesophotic reef hydrodynamic processes appear to be less of a factor in sediment deposition when compared to shallower-water reef systems (Randazzo and Baisley, 1995; Orpin et al., 1999; Storlazzi et al., 2004). Significant terrigenous material, easily distinguished from reef carbonates, was found exclusively at the shallowest sites. This suggests that some portion of the land-based siliciclastic input often associated with and transported as terrigenous sediment may still be affecting the near-shore reef system (Gray et al., 2008), but is not likely to have a direct effect on mesophotic sites.

Sand-sized sediments at mesophotic reef habitats in the USVI do not experience significant transport between sites, and do not experience gravity-driven sediment movement possible in steeper systems. This is observed by comparing models of suspended particles to sediment trap deposits. Though almost never theoretically depositing at any mesophotic reef sites during average spring–neap tidal cycle current velocity mean conditions, suspended particles with diameters ≥104.4 μm (mean grain diameter collected in Hind Bank sediment traps 1.36 km from D2; Smith et al., 2008) had potential to deposit at the Deep Patch site during 26. 21% of the measured hours, provided the grains were in the water column. However, sedimentation trap rates near the Deep Patch were seven times lower than at the Fringing Patch (D2: 0.315 mg/cm^2/day, standard error = 0.037; S6: 2.315 mg/cm^2/day, standard error = 0.327; Smith et al., 2008). Therefore, particles with diameters ≥104.4 μm were either scarce at neighboring sources (though not the case for neighboring mesophotic reefs; Fig. 2a), or current energy was not sufficient to sustain transport of these grain sizes from other sources to the Deep Patch. Assuming similar external sediment sources, sedimentation rates at the other mesophotic reefs would be comparable to those recorded near the Deep Patch and imply that sand-sized sediment at all analyzed mesophotic reef sites have predominately localized origins.

Although biological processes appear to be the primary control of sediment characteristics at USVI mesophotic reefs, entrainment potential for fine sand grains and smaller allow for some interpretation of hydrodynamic conditions in the mesophotic reef sedimentary record. USVI mesophotic reef sediments have different potential for entrainment per habitat when responding to average spring–neap tidal cycle current velocity maximum; potential mobility generally increases with higher speeds. Grain size analysis, low sedimentation rates, and potential mobility analysis indicates that in 1 year, production/deposition of fine sand grains and smaller (≤0.203 mm) was less frequent at the Deep Patch than the 22 h of the year (0.26%) in which conditions would be able to cause at least 10% potential mobility to remove most fine grains (Fig. 5). However, this hydrodynamic activity was probably not high enough to physically break down calcareous green algae, the most abundant grain type in the surface sediments at the Deep Patch (Fig. 2) and one of the quickest reef skeletal grain types to disassociate (Ford and Kench, 2012). Contrastingly, potential mobility analysis indicates that faster, more frequent episodic currents may be responsible for breaking up and removing sediment generated from the moderate calcareous green algae benthic cover at the Hillock Basin site, reducing the mean grain size. This is also supported by the fact that plate-shaped *Halimeda* grains tend to behave hydraulically as smaller particles compared to coral grains (Kench and McLean, 1997).

The low proportion of mud and fine-grained sand in MCE reef sediments, especially equivalent in size to average sponge chips (Fig. 4c), also indicates hydrodynamic conditions have some influence on USVI mesophotic reef sedimentology. The relative absence is not intuitive because sponge bioerosion is considered the primary long-term modifier of substrate below ~ 35 m (Weinstein et al., 2014). USVI mesophotic reef coral sponge bioerosion is either cryptic or primarily on the underside of platy coral heads. Expelled chips from less-cryptic sponges must fall before autochthonous deposition. However, energy levels were almost never low enough (<1.50% of measured hours; Table 3) for potential deposition of equivalent-sized particles, assuming fall heights ≥25 mm, or for long-term residence on the surface. A greater abundance of sponge chips is expected in cryptic spaces, but these may not mix into surrounding surface sediment where samples were collected. Therefore, although sponge chips can constitute a high percent of reef sediment in low energy habitats (such as lagoons; Fütterer, 1974), there is little potential for sponge chip accumulation on low-angle shelf MCEs due to moderately strong episodic hydrodynamic forces.

A byproduct of hydrodynamic removal of sponge chips from USVI mesophotic reefs is the high probability that most all other generation of coral-based sediment occurs through parrotfish grazing. Therefore, another implication from this study is that sediment analysis in upper mesophotic reefs along low-angle slopes can be used to infer past grazing bioerosional productivity. This is important considering macroboring analysis in fossil reefs is possible but few reliable methods exist for estimating grazing contributions to total bioerosion in the same deposits.

Further interpretation of hydrodynamic impacts on sediment characteristics in the USVI is not possible. This results from the observation that average spring–neap tidal cycle current velocity means are relatively similar (Table 1) and that different sites can appear to experience greater current depending on the interval of time measured (Smith et al., 2010). Additional limitations to detect hydrodynamic patterns depend on how effective our methods were in correcting problems associated with applying carbonate sediment sieve-based grain size analysis to hydrodynamic interpretations (Kench and McLean, 1997).

4.3. Implications for comparative analysis

Low diversity in grain producers has been suggested to result in reduced sedimentary facies variability in reefs at MCE depth ranges compared to their shallow-water reef counterparts (Purkis et al., 2015). However, our findings indicate distinct associations between deep reef habitats with architecturally different characteristics and sedimentary subfacies (Table 2). Results imply reservoir models of carbonate deposits from ancient mesophotic reef settings could be refined to better reflect heterogeneity of sediment properties. The present study suggests mesophotic reef habitat heterogeneity in the USVI can be distinguished based on sedimentological data. This is critical for future comparative studies of mesophotic reef paleoenvironments, especially considering that mesophotic reef systems like those examined in the USVI may often be dominated by one major taxonomic coral group. Although many studies have used key species, growth forms, or ecological zonation to interpret reef paleoenvironments (Mesolella et al., 1970; Chappell, 1974; Lighty et al., 1982), there is a risk of circular reasoning error when relying on these sole factors to both interpret paleoenvironmental conditions and paleoecology from the same samples (Pandolfi et al., 1999).

The subfacies identified do not necessarily represent characteristics completely unique to mesophotic reef habitats. However, they allow for a more comprehensive interpretation of benthic ecology and hydrological conditions experienced at mesophotic reefs with different geomorphological habitats. They can also help determine the degree of habitat heterogeneity in the particular reef system, different reef environments, and the lateral extent of different reef habit types. Regardless, consideration is still needed when interpreting ancient mesophotic reef deposits. Based on mean grain sizes, the classical fluid sediment transport theory (smaller grains identify areas of reduced energy and larger grains identify areas of greater energy; Purdy, 1963) would lead, incorrectly, to the interpretation that the Deep Patch is a higher energy environment than the Hillock Basin. Identifying high abundance of very fine grain reef sediment in ancient mesophotic reef deposits should not be the only observation used to imply a Hillock Basin-type environment. Interpreting other factors such as bedding structures, syndepositional cement, bioturbation, and amount of allochthonous material is necessary before subfacies equivalence can be inferred. These additional indicators, as well as the grain composition, would help identify if smaller size grains resulted from low energy, or if higher relative average spring–neap tidal cycle current velocity maximum conditions were possible, such as those experienced at the Hillock Basin. At the least, we suggest that similar paleomesophotic reef subfacies delineations to those in the USVIs would indicate a high probability of MCE depth shelf-wide habitat heterogeneity that may otherwise have been overlooked. Results from this study provide a new analog for studying mesophotic reef systems in the geologic past and overall coral reef evolution.

Supplementary data to this article can be found online at http://dx.doi.org/10.1016/j.sedgeo.2015.07.003.

Acknowledgments

We thank P. Swart for geochemical support and interpretations, P. Reid, R. Ginsburg, and D. McNeill for guidance and early manuscript comments, and A. Shansby, J. Weinstein, and R. Cunning for early conceptualization. Technical diving and field support was provided by R. Gomez, E. Kadison, and M. Kammann. Assistance with laboratory analyses was provided by C. Kaiser, R. Thompson, C. Gil, and S. Dowiarz. A. Weinstein provided editorial review. Funding was provided by the National Science Foundation, Sigma Xi, the Geological Society of America, ExxonMobil, the Academy of Underwater Arts and Sciences, the University of Miami Center for Latin American Studies, the Leonard and Jayne Abess/Citizens Board, and the RSMAS Graduate Student Fund. This is contribution # 126 from the Center for Marine and Environmental Studies, UVI.

References

Abbey, E., Webster, J.M., Braga, J.C., Jacobsen, G.E., Thorogood, G., Thomas, A.L., Camoin, G., Reimer, P.J., Potts, D.C., 2013. Deglacial mesophotic reef demise on the Great Barrier Reef. Palaeogeography, Palaeoclimatology, Palaeoecology 392, 473–494.

Adams, A.E., Mackenzie, W.S., Guilford, C., 1984. Atlas of Sedimentary Rocks Under the Microscope. Longman Scientific and Technical, Essex, England.

Baker, A.C., Starger, C.J., McClanahan, T.R., Glynn, P.W., 2004. Coral reefs: corals' adaptive response to climate change. Nature 430 (7001), 741.

Basan, P.B., 1973. Aspects of sedimentation and development of a carbonate bank in the Barracuda Keys, south Florida. Journal of Sedimentary Petrology 43 (1), 42–53.

Blott, S.J., Pye, K., 2001. Gradistat: a grain size distribution and statistics package for the analysis of unconsolidated sediments. Earth Surface Processes and Landforms 26, 1237–1248.

Boss, S.K., Liddell, W.D., 1987. Patterns of sediment composition of Jamaican fringing reef facies. Sedimentology 34 (1), 77–87.

Bozec, Y., Alvarez-Filip, L., Mumby, P.J., 2014. The dynamics of architectural complexity on coral reefs under climate change. Global Change Biology 21, 223–235.

Bridge, T., Fabricius, K., Bongaerts, P., Wallace, C., Muir, P., Done, T., Webster, J., 2012. Diversity of Scleractinia and Octocorallia in the mesophotic zone of the Great Barrier Reef, Australia. Coral Reefs 31 (1), 179–189.

Bruno, J.F., Bertness, M.D., 2001. Habitat modification and facilitation in benthic marine communities. In: Bertness, M.D., Gaines, S.D., Hay, M.E. (Eds.), Marine Community Ecology. Sinaur, Sunderland, MA, pp. 201–218.

Cerrano, C., Danovaro, R., Gambi, C., Pusceddu, A., Riva, A., Schiaparelli, S., 2010. Gold coral (*Savalia savaglia*) and gorgonian forests enhance benthic biodiversity and ecosystem functioning in the mesophotic zone. Biodiversity and Conservation 19 (1), 153–167.

Chappell, J., 1974. Geology of coral terraces, Huon Peninsula, New Guinea: a study of Quaternary tectonic movements and sea-level changes. Geological Society of America Bulletin 85 (4), 553–570.

Cheng, N., Chiew, Y., 1999. Analysis of initiation of sediment suspension from bed-load. Journal of Hydraulic Engineering 125 (8), 855–861.

Connell, J.H., 1978. Diversity in tropical rain forests and coral reefs. Science 199 (4335), 1302–1310.

Craig, H., 1957. Isotopic standards for carbon and oxygen and correction factors for mass-spectrometric analysis of carbon dioxide. Geochimica et Cosmochimica Acta 12 (1), 133–149.

Dill, M.A., Seyrafian, A., Vaziri-Moghaddam, H., 2012. Palaeoecology of the Oligocene–Miocene Asmari Formation in the Dill Anticline (Zagros Basin, Iran). Neues Jahrbuch für Geologie und Paläontologie Abhandlungen 263 (2), 167–184.

Dryden, C., Cortes, J., Newman, S., Sanchez, C., Williams, S., Polunin, N., 2012. Future of reefs in a changing environment: an ecosystem approach to managing Caribbean coral reefs in the face of climate change. Preliminary Report on the Relationship between Architectural Complexity and Reef Biodiversity, p. 10.

Dustan, P., Doherty, O., Pardede, S., 2013. Digital reef rugosity estimates coral reef habitat complexity. PLoS ONE 8 (2), e57386.

Eckman, J.E., Duggins, D.O., Sewell, A.T., 1989. Ecology of under story kelp environments. I. Effects of kelps on flow and particle transport near the bottom. Journal of Experimental Marine Biology and Ecology 129 (2), 173–187.

El-Dessouky, E., Ettouney, H., 2002. Fundamentals of Salt Water Desalination (Appendix A: Themodynamic Properties). Elsevier, New York.

Flood, P.G., Scoffin, T.P., 1978. Reefal sediments of the Northern Great Barrier Reef. Philosophical Transactions of the Royal Society of London, Series A: Mathematical and Physical Sciences 291 (1378), 55–68.

Flügel, E., Flügel-Kahler, E., 1992. Phanerozoic reef evolution: basic questions and data base. Facies 26 (1), 167–277.

Folk, R.L., 1974. Petrology of Sedimentary Rocks. The Walter Geology Library, Austin, Texas.

Folk, R.L., Robles, R., 1964. Carbonate sands of Isla Perez, Alacran Reef Complex, Yucatan. The Journal of Geology 72 (3), 225–291.

Ford, M.R., Kench, P.S., 2012. The durability of bioclastic sediments and implications for coral reef deposit formation. Sedimentology 59 (3), 830–842.

Fricke, H.W., Vareschi, E., Schlichter, D., 1987. Photoecology of the coral *Leptoseris fragilis* in the Red Sea twilight zone (an experimental study by submersible). Oecologia 73 (3), 371–381.

Fütterer, D.K., 1974. Significance of the boring sponge *Cliona* for the origin of fine grained material of carbonate sediments. Journal of Sedimentary Petrology 44 (1), 79–84.

Garrett, P., Smith, D.L., Wilson, A.O., Patriquin, D., 1971. Physiography, ecology, and sediments of two Bermuda patch reefs. Journal of Geology 79 (6), 647–668.

Gibbs, R.J., Matthews, M.D., Link, D.A., 1971. The relationship between sphere size and settling velocity. Journal of Sedimentary Petrology 41 (1), 7–18.

Ginsburg, R., 1956. Environmental relationships of grain size and constituent particles in some South Florida carbonate sediments. AAPG Bulletin 40 (10), 2384–2427.

Gischler, E., Swart, P.K., Lomando, A.J., 2009. Stable isotopes of carbon and oxygen in modern sediments of carbonate platforms, barrier reefs, atolls and ramps: Patterns and implications. In: Swart, P.K., Eberli, G.P., McKenzie, J.A., Jarvis, I., Stevens, T. (Eds.), Perspectives in Carbonate Geology: A Tribute to the Career of Robert Nathan Ginsburg. John Wiley & Sons, Ltd., Chichester, West Sussex, UK, pp. 61–74.

Gray, S.C., Gobbi, K.L., Narwold, P.V., 2008. Comparison of sedimentation in bays and reefs below developed versus undeveloped watersheds on St. John, U.S. Virgin Islands. pp. 351–356.

Gygi, R.A., 1969. An estimate of the erosional effect of *Sparisoma viride* (Bonnaterre), the green parrotfish, on some Bermuda reefs. In: Ginsburg, R.N., Garrett, P. (Eds.), Reports of Research: 1968 Seminar on Organism–Sediment Interrelationships, Bermuda Biological Station for Research, pp. 137–143.

Hammer, Ø., Harper, D.A.T., Ryan, P.D., 2001. PAST: paleontological statistics software package for education and data analysis. Palaeontologia Electronica 4 (1), 9.

Hutchings, P.A., 1986. Biological destruction of coral reefs. Coral Reefs 4, 239–252.

Insalaco, E., 1996. Upper Jurassic microsolenid biostromes of northern and central Europe: facies and depositional environment. Palaeogeography, Palaeoclimatology, Palaeoecology 121 (3–4), 169–194.

Jordan, C.F., 1973. Carbonate facies and sedimentation of patch reefs off Bermuda. AAPG Bulletin 57 (1), 42–54.

Kench, P.S., 1998. A currents of removal approach for interpreting carbonate sedimentary processes. Marine Geology 145 (3–4), 197–223.

Kench, P.S., McLean, R.F., 1996. Hydraulic characteristics of bioclastic deposits: new possibilities for environmental interpretation using settling velocity fractions. Sedimentology 43 (3), 561–570.

Kench, P.S., McLean, R.F., 1997. A comparison of settling and sieve techniques for the analysis of bioclastic sediments. Sedimentary Geology 109 (1), 111–119.

Komar, P.D., 1981. The applicability of the Gibbs equation for grain settling velocities to conditions other than quartz grains in water. Journal of Sedimentary Petrology 51 (4), 1125–1132.

Lesser, M.P., Slattery, M., Leichter, J.J., 2009. Ecology of mesophotic coral reefs. Journal of Experimental Marine Biology and Ecology 375 (1-2), 1–8.

Lesser, M.P., Slattery, M., Stat, M., Ojimi, M., Gates, R.D., Grottoli, A., 2010. Photoacclimatization by the coral *Montastraea cavernosa* in the mesophotic zone: light, food, and genetics. Ecology 91 (4), 990–1003.

Lidz, B.H., Hallock, P., 2000. Sedimentary petrology of a declining reef ecosystem, Florida Reef Tract (U. S. A.). Journal of Coastal Research 16 (3), 675.

Lighty, R.G., Macintyre, I.G., Stuckenrath, R., 1982. *Acropora palmata* reef framework: a reliable indicator of sea level in the western Atlantic for the past 10,000 years. Coral Reefs 1 (2), 125–130.
Luckhurst, B.E., Luckhurst, K., 1978. Analysis of the influence of substrate variables on coral reef fish communities. Marine Biology 49 (4), 317–323.
Mateu-Vicens, G., Pomar, L., Ferràndez-Cañadell, C., 2012. Nummulitic banks in the upper Lutetian 'Buil level', Ainsa Basin, South Central Pyrenean Zone: the impact of internal waves. Sedimentology 59 (2), 527–552.
May, J.P., 1981. Chi (x): a proposed standard parameter for settling tube analysis of sediments. Journal of Sedimentary Petrology 51 (2), 607–610.
Mesolella, K.J., Sealy, H.A., Matthews, R.K., 1970. Facies geometries within Pleistocene reefs of Barbados, West Indies. The American Association of Petroleum Geologists Bulletin 54 (10), 1899–1917.
Mihaljević, M., Renema, W., Welsh, K., Pandolfi, J.M., 2014. Eocene–Miocene shallow-water carbonate platforms and increased habitat diversity in Sarawak, Malaysia. Palaios 29, 378–391.
Millero, F.J., Chen, C., Bradshaw, A., Schleicher, K., 1980. A new high pressure equation of state for seawater. Deep Sea Research Part A: Oceanographic Research Papers 27 (3–4), 255–264.
Morsilli, M., Bosellini, F.R., Pomar, L., Hallock, P., Aurell, M., Papazzoni, C.A., 2012. Mesophotic coral buildups in a prodelta setting (Late Eocene, southern Pyrenees, Spain): a mixed carbonate-siliciclastic system. Sedimentology 59 (3), 766–794.
Novak, V., Santodomingo, N., Rösler, A., Di Martino, E., Braga, J.C., Taylor, P.D., Johnson, K.G., Renema, W., 2013. Environmental reconstruction of a late Burdigalian (Miocene) patch reef in deltaic deposits (East Kalimantan, Indonesia). Palaeogeography, Palaeoclimatology, Palaeoecology 374, 110–122.
Orpin, A.R., Ridd, P.V., Stewart, L.K., 1999. Assessment of the relative importance of major sediment transport mechanisms in the central Great Barrier Reef lagoon. Australian Journal of Earth Sciences 46 (6), 883–896.
Pandolfi, J.M., Llewellyn, G., Jackson, J.B.C., 1999. Pleistocene reef environments, constituent grains, and coral community structure: Curaçao, Netherlands Antilles. Coral Reefs 18 (2), 107–122.
Perry, C., 1996. The rapid response of reef sediments to changes in community composition; implications for time averaging and sediment accumulation. Journal of Sedimentary Research 66 (3), 459–467.
Prager, E.J., Southard, J.B., Vivoni-Gallart, E.R., 1996. Experiments on the entrainment threshold of well-sorted and poorly sorted carbonate sands. Sedimentology 43 (1), 33–40.
Purdy, E.G., 1963. Recent calcium carbonate facies of the Great Bahama Bank. 1. Petrography and reaction groups. Journal of Geology 71 (3), 334–355.
Purkis, S.J., Rowlands, G.P., Kerr, J.M., 2015. Unravelling the influence of water depth and wave energy on the facies diversity of shelf carbonates. Sedimentology 62 (2), 541–565.
Pusey, W.C., 1975. Holocene carbonate sedimentation on Northern Belize Shelf: Part 1. In: Wantland, K.L., Pusey, W.C. (Eds.), Belize Shelf — Carbonate Sediments, Clastic Sediments, and Ecology. AAPG Studies in Geology, Tulsa, Oklahoma, pp. 131–165.
R Core Team, 2014. R: A Language and Environment for Statistical Computing.
Randazzo, A.F., Baisley, K.J., 1995. Controls on carbonate facies distribution in a high-energy lagoon, San Salvador Island, Bahamas. Geological Society of America, Special Paper 300, 157–175.
Renema, W., Bellwood, D.R., Braga, J.C., Bromfield, K., Hall, R., Johnson, K.G., Lunt, P., Meyer, C.P., McMonagle, L.B., Morley, R.J., O'Dea, A., Todd, J.A., Wesselingh, F.P., Wilson, M.E.J., Pandolfi, J.M., 2008. Hopping hotspots: global shifts in marine biodiversity. Science 321 (5889), 654–657.
Roberts, C.M., Ormond, R.F.G., 1987. Habitat complexity and coral reef fish diversity and abundance on Red Sea fringing reefs. Marine Ecology Progress Series 41 (1), 1–8.
Roduit, N., 2008. JMicroVision: Image Analysis Toolbox for Measuring and Quantifying Components of High-definition Images (accessed 11/12/2013).
Rosen, B.R., Aillud, G.S., Bosellini, F.R., Clack, N.J., Insalaco, E., Valldeperas, F.X., Wilson, M.E.J., 2000. Platy Coral Assemblages: 200 Million Years of Functional Stability in Response to the Limiting Effects of Light and Turbidity. pp. 255–264.
Rützler, K., 1975. The role of burrowing sponges in bioerosion. Oecologia 19 (3), 203–216.
Scholle, P.A., 1978. A Color Illustrated Guide to Carbonate Rock Constituents, Textures, Cements, and Porosities. American Association of Petroleum Geologists, Tulsa, Oklahoma.
Scoffin, T.P., 1992. Taphonomy of coral reefs: a review. Coral Reefs 11 (2), 57–77.
Scoffin, T.P., Tudhope, A.W., 1985. Sedimentary environments of the central region of the Great Barrier Reef of Australia. Coral Reefs 4 (2), 81–93.
Smith, T.B., Nemeth, R.S., Blondeau, J., Calnan, J.M., Kadison, E., Herzlieb, S., 2008. Assessing coral reef health across onshore to offshore stress gradients in the US Virgin Islands. Marine Pollution Bulletin 56, 1983–1991.
Smith, T.B., Blondeau, J., Nemeth, R.S., Pittman, S.J., Calnan, J.M., Kadison, E., Gass, J., 2010. Benthic structure and cryptic mortality in a Caribbean mesophotic coral reef bank system, the Hind Bank Marine Conservation District, U.S. Virgin Islands. Coral Reefs 29 (2), 289–308.
Soulsby, R., 1997. Dynamics of Marine Sands. Thomas Telford Publications, London.
Stanley, G.D., Fautin, D.G., 2001. Palenotology and evolution: the origins of modern corals. Science 291 (5510), 1913–1914.
Storlazzi, C.D., Ogston, A.S., Bothner, M.H., Field, M.E., Presto, M.K., 2004. Wave- and tidally-driven flow and sediment flux across a fringing coral reef: Southern Molokai, Hawaii. Continental Shelf Research 24 (12), 1397–1419.
Swart, P.K., Burns, S.J., Leder, J.J., 1991. Fractionation of the stable isotopes of oxygen and carbon in carbon dioxide during the reaction of calcite with phosphoric acid as a function of temperature and technique. Chemical Geology 86 (2), 89–96.
Thompson, R.C., Wilson, B.J., Tobin, M.L., Hill, A.S., Hawkins, S.J., 1996. Biologically generated habitat provision and diversity of rocky shore organisms at a hierarchy of spatial scales. Journal of Experimental Marine Biology and Ecology 202 (1), 73–84.
Veron, J.E.N., 1995. Corals in Space and Time: Biogeography and Evolution of the *Scleractinians*. Cornell University Press, Ithaca, NY.
Weinstein, D.K., Klaus, J.S., Smith, T.B., 2014. Mesophotic bioerosion: variability and structural impact on U.S. Virgin Island deep reefs. Geomorphology 222, 14–24.